Type-I superconductivity in the Dirac semimetal PdTe$_2$

H. Leng,[1,*] C. Paulsen,[2] Y. K. Huang,[1] and A. de Visser[1,†]

[1]*Van der Waals–Zeeman Institute, University of Amsterdam, Science Park 904, 1098 XH Amsterdam, The Netherlands*
[2]*Institut Néel, CNRS & Université Grenoble Alpes, BP 166, 38042 Grenoble Cedex 9, France*

The superconductor PdTe$_2$ was recently classified as a type-II Dirac semimetal, and advocated to be an improved platform for topological superconductivity. Here, we report magnetic and transport measurements conducted to determine the nature of the superconducting phase. Surprisingly, we find that PdTe$_2$ is a type-I superconductor with $T_c = 1.64$ K and a critical field $\mu_0 H_c(0) = 13.6$ mT. Our crystals also exhibit the intermediate state as demonstrated by the differential paramagnetic effect. For $H > H_c$ we observe superconductivity of the surface sheath. This calls for a close examination of superconductivity in PdTe$_2$ in view of the presence of topological surface states.

Recently, the transition metal dichalcogenide PdTe$_2$ was reported to be a type-II Dirac semimetal [1–3]. Topological Dirac semimetals form a new class of topological materials, where nontrivial surface states arise due to the topology of the bulk band structure (for recent reviews, see Refs. [4–6]). Dirac semimetals are the three-dimensional (3D) analog of graphene and have a cone-shaped linear energy dispersion around the Dirac point with massless fermions [7]. The bands have a double degeneracy that can be lifted by a magnetic field resulting in a pair of Weyl cones. In the closely related class of Weyl semimetals, the degeneracy is naturally lifted by breaking time reversal and/or inversion symmetry [8]. The set of Weyl cones can give rise to distinct properties, such as Fermi arcs at the surface, a quantum anomalous Hall effect, and chiral magnetotransport [5,6]. Type-I Dirac semimetals are similar to graphene and the valence and conduction bands meet at the Dirac point and Lorentz invariance is obeyed. In type-II Dirac semimetals an extra momentum-dependent term in the Hamiltonian breaks Lorentz invariance [9–11]. This can be accomplished by tilting the Dirac cone, where the Dirac point is now the touching point of the electron and hole pockets. This gives rise to a number of new physical phenomena, such as an angle-dependent chiral anomaly and topological Lifshitz transitions [5,6].

Superconductivity in PdTe$_2$ with a transition temperature T_c of 1.5 K was discovered in 1961 [12]. The recent detection of topological features in the band structure raises the question whether superconductivity has also a topological nature [1,2,13]. Notably, it has been advocated that PdTe$_2$ is an improved platform for topological superconductivity [2]. Topological superconductors attract much attention because they are predicted to host protected Majorana zero modes at their surface (for recent reviews, see Refs. [14,15]). This offers a unique design route to produce future devices for topological quantum computation. Unfortunately, the number of materials in which topological superconductivity has been realized – or is under debate – is very small [15]. Majorana modes, which appear as gapless nodes in the bulk superconducting gap, are in general not stable in a type-I Dirac semimetal [15]. However,

in a type-II semimetal the situation is different because of the tilted dispersion. Moreover, the abundance of states in the electron and hole pockets near the type-II Dirac point favors a larger carrier concentration and superconductivity [2].

Hitherto, the superconducting state of PdTe$_2$ has yet to be studied in detail. The early determination of T_c by Guggenheim *et al.* [12] was confirmed by others with T_c values ranging from 1.7 to 2.0 K [2,16–18]. Fei *et al.* [2] investigated the depression of T_c in magnetic field and reported an anomalous upward curvature of the upper critical field $H_{c2}(T)$ with $\mu_0 H_{c2} = 0.32$ T for $T \to 0$. In view of the proposed topological nature of the superconducting state [1,2,13], an in-depth characterization of the superconducting phase is a matter of great urgency. Here, we report magnetic and transport measurements on single crystals that unambiguously show PdTe$_2$ is a type-I superconductor. This makes PdTe$_2$ a topological material where superconductivity is of type I. This is a surprising result, also because the number of known binary and ternary systems with type-I superconductivity is very small (see, for instance, Refs. [19–21] and references therein). Our crystals also show enhanced superconductivity of the surface sheath in fields exceeding the critical field H_c. The surface superconductivity does not obey the standard Saint-James–de Gennes behavior with critical field $H_{c3} = 2.39 \times \kappa H_c$ [22,23]. We discuss these unusual results in view of the presence of topological surface states [1,13].

PdTe$_2$ crystallizes in the trigonal CdI$_2$ structure (space group $P\bar{3}m1$) [24]. It belongs to the family of transition metal dichalcogenides, which is intensively studied because of the remarkable physical properties [25]. Its normal-state electronic properties have been investigated in the 1970's by quantum oscillation experiments and band-structure calculations [26–28]. The topological nature of the electronic band structure was reported recently [1,2,13]. Notably, angle-resolved photoemission spectroscopy (ARPES) combined with *ab initio* band-structure calculations revealed PdTe$_2$ is a type-II Dirac semimetal [1], which finds further support in a nontrivial Berry phase originating from a hole pocket formed by a tilted Dirac cone [2]. The fundamental electronic properties of PdTe$_2$ were revisited recently by transport, magnetic, and thermal measurements [29].

For our study of the superconducting properties of PdTe$_2$ we prepared a single crystal by a modified Bridgman tech-

———————
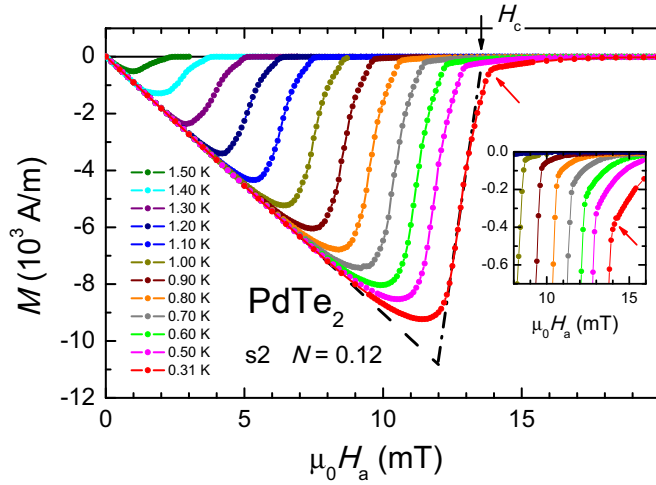*h.leng@uva.nl
†a.devisser@uva.nl

FIG. 1. dc magnetization per unit volume (SI units) as a function of applied field for PdTe$_2$ at temperatures from 0.31 K (right) to 1.50 K (left), as indicated. The initial slope $\chi_m = dM/dH_a$ accounts for a superconducting sample volume of 100% with $N = 0.12$ (dashed line). The dashed-dotted line indicates the idealized $M(H_a)$ curve with slope $1/N$ in the intermediate state at $T = 0.31$ K. The black arrow indicates H_c at $T = 0.31$ K. The red arrow points to a kink and start of a tail in $M(H_a)$. Inset: Zoom of the kink feature at a few selected temperatures.

nique [30]. Powder x-ray diffraction confirmed the CdI$_2$ structure. Scanning electron microscopy (SEM) with energy dispersive x-ray (EDX) spectroscopy showed the proper 1:2 stoichiometry within the experimental resolution of 0.5% (see Supplemental Material (SM) [31]). Laue backscattering was used to orient the crystal. Single-crystalline bars, typically a few mm long, were cut along the crystallographic a axis by means of a scalpel blade and/or spark erosion. Standard four-point resistance measurements were carried out in a physical property measurement system (Quantum Design) at temperatures down to 2 K and in a ^{3}He refrigerator (Heliox, Oxford Instruments) down to 0.3 K. dc magnetization $M(T,H)$ and ac susceptibility $\chi_{ac}(T,H)$ measurements were made using a low-field superconducting quantum interference device (SQUID) magnetometer developed at the Néel Institute. The magnetometer is equipped with a miniature dilution refrigerator making possible absolute value measurements by the extraction technique. A MuMetal and superconducting shield combination results in a residual field of a few mOe at the sample position when cooled. As regards χ_{ac}, the in-phase χ'_{ac} and out-of-phase χ''_{ac} signals were measured in driving fields $\mu_0 H_{ac} = 0.0005$–0.25 mT with low frequencies $f_{ac} = 2.3$–13 Hz.

In Fig. 1 we show the dc magnetization as a function of the applied field H_a in the temperature range 0.31–1.50 K. The $M(H_a)$ curves follow the behavior of a type-I superconductor with a Meissner phase up to $\mu_0 H_a = 12$ mT and the intermediate state for 12 mT $< \mu_0 H_a < \mu_0 H_c = 13.6$ mT, where H_c is the critical field. The large value of the measured initial slope $\chi_m = dM/dH_a = \chi(1 + N\chi) = -1.13$ is in agreement with bulk superconductivity. Here, N is the demagnetization factor and $\chi = -1$ the ideal susceptibility [32]. From the initial slope we calculate $N = 0.12$, which is close to the estimated value
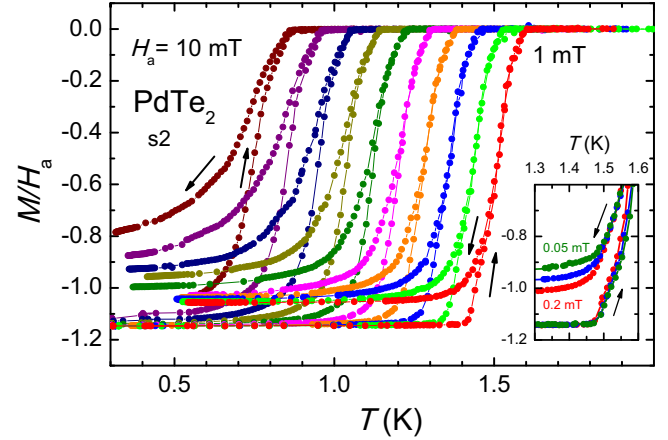

FIG. 2. dc susceptibility M/H_a (in SI units) as a function of temperature in fields $\mu_0 H_a$ from 1 mT (right) to 10 mT (left) in steps of 1 mT. Data are taken after cooling in zero field (ZFC) and field cooled (FC) as shown by the arrows. Inset: Part of the ZFC-FC curves in applied fields of 0.2 (red), 0.1 (blue), and 0.05 mT (green).

$\sim$0.10 based on the sample shape (see SM [31]). We remark the rounding of the curves is due to the nonuniform magnetization at the sample edges. However, a clear kink and tail is observed in the data just above H_c (see inset). We will return to this point later. We have determined $H_c(T)$ by extrapolating the idealized linear $M(H_a)$ curves to $M = 0$, as shown by the dashed-dotted line for $T = 0.31$ K in Fig. 1. The critical field follows the standard BCS quadratic temperature variation $H_c(T) = H_c(0)[1 - (T/T_c)^2]$, with $\mu_0 H_c = 13.6$ mT and $T_c = 1.64$ K (see Fig. 4).

The temperature variation of the dc susceptibility $\chi_{dc}(T)$ in applied fields $\leqslant 10$ mT is shown in Fig. 2. The data are taken after cooling in zero field (ZFC) and field cooled (FC). The FC data at low applied dc fields ($\mu_0 H_a = 1$ mT) demonstrate a large Meissner effect with a flux expulsion of 93 %. We remark that for very small dc fields $\leqslant 0.2$ mT, flux expulsion is reduced (85% in 0.05 mT), as shown in the inset of Fig. 2. ac susceptibility measurements in an ac driving field $\mu_0 H_{ac} = 0.25$ mT for dc fields up to 10 mT are reported in Figs. 3(a) and 3(b). At low temperatures, χ'_{ac} shows a full superconducting screening signal. Upon increasing the temperature, χ'_{ac} does not show the usual smooth increase to zero. Instead, the signal becomes positive and shows a large peak before the normal state is reached at T_c. This is known as the differential paramagnetic effect (DPE) [33]. It results from the positive $\partial M/\partial H_a$ below H_c in the intermediate state (see Fig. 1), i.e., in between $(1 - N)H_c$ and H_c, and has been observed in other type-I superconductors as well [19,21]. $H_c(T)$ data points extracted from the dc and ac susceptibility data in fixed fields have been collected in Fig. 4 as well.

The dc magnetization, the ac susceptibility with DPE, and the extracted T^2 variation of H_c all provide solid evidence that PdTe$_2$ is a type-I superconductor. This tells us the Ginzburg-Landau parameter $\kappa = \lambda/\xi < 1/\sqrt{2}$. An estimate for the magnetic penetration depth λ can be obtained using the London equation $\lambda = (m^*/\mu_0 n_s e^2)^{1/2}$, where m^* is the effective mass, n_s the superfluid density, and e the elementary charge. With a carrier density $n = 5.5 \times 10^{27}$ m^{-3} determined by Hall effect
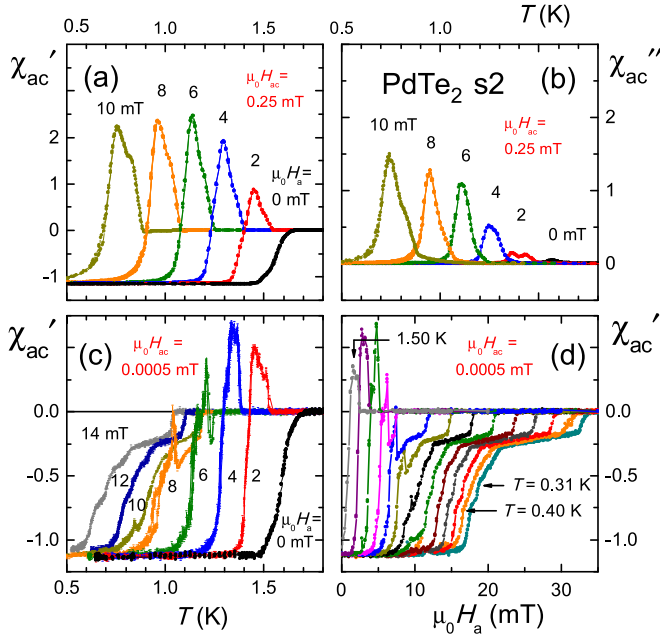
FIG. 3. ac susceptibility of PdTe$_2$. Upper panels (a) and (b): In-phase and out-of-phase component of the ac susceptibility for an ac driving field $\mu_0 H_{ac} = 0.25$ mT. Data are taken in dc fields $\mu_0 H_a = 0$–10 mT, as indicated. The large peaks in χ'_{ac} when a dc field is applied are due to the differential paramagnetic effect. Lower panels: ac susceptibility in a small ac driving field $\mu_0 H_{ac} = 0.0005$ mT. (c) As a function of temperature at dc fields from 0 to 14 mT, as indicated. (d) As a function of applied field at a temperature of 0.31 K, and from 0.40 to 1.50 K in steps of 0.1 K.

measurements on our crystals, and $m^* \approx 0.3 m_e$ [18,27] (here, we use an average value m^* and m_e is the free-electron mass), we calculate $\lambda \approx 39$ nm. A value for the superconducting coherence length ξ can be derived from the Ginzburg-Landau relation $\xi = \Phi_0 / (2\sqrt{2}\pi\mu_0 H_c \lambda)$ [34], where Φ_0 is the flux quantum. With the measured value $H_c(0) = 13.6$ mT, we obtain $\xi \approx 114$ nm, and calculate $\kappa \approx 0.34$. We remark that realistic error margins in the values of n and m^* will not affect the result $\kappa < 1/\sqrt{2}$. A value for $\kappa \leqslant 0.42$ is further supported by the observation of supercooling (see Fig. S7(a) in SM [31]). Supercooling is predicted to occur for $\kappa \leqslant 0.42$, and is manifest in magnetization measurements in decreasing fields, where the sample remains in the normal state below H_c [23,34]. Since $-\mu_0 H_c^2/2$ is the condensation energy per unit volume, we can use thermodynamic relations to calculate H_c from the step size of the specific heat at T_c using the relation $\Delta C|_{T_c} = 4\mu_0 H_c(0)^2/T_c = 1.43 \times \gamma T_c$ [32], assuming PdTe$_2$ is a weak-coupling BCS superconductor [35]. Here, γ is the Sommerfeld coefficient. With the experimental value $\gamma = 138$ J/K^2 m^3 [29,35] (the molar volume is 4.34×10^{-5} m^3/mol), we calculate $\mu_0 H_c(0) = 12.6$ mT, which is close to the measured value reported in Fig. 4.

Having established that PdTe$_2$ is a bulk type-I superconductor, we next turn to superconductivity of the surface sheath. A close inspection of the $M(H)$ isotherms reported in Fig. 1 reveals a clear kink in the data close to H_c and a long tail for $M(H) \to 0$ (see the inset). Thus superconductivity survives above H_c. This is also most clearly observed in
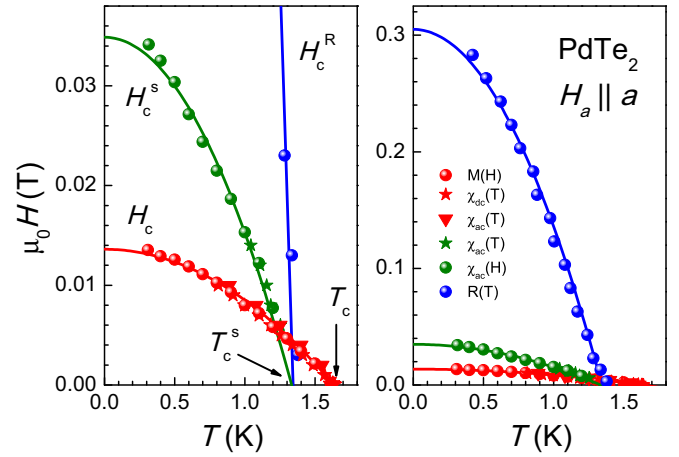

FIG. 4. Superconducting phase diagram of PdTe$_2$ for $H_a \parallel a$ axis. Bulk superconductivity is found below $H_c(T)$ as determined by dc magnetization and χ'_{ac}. The red line represents a fit to $H_c(T) = H_c(0)[1 - (T/T_c)^2]$, with $\mu_0 H_c(0) = 13.6$ mT and $T_c = 1.64$ K. Surface superconductivity is found below $H_c^s(T)$ as determined by χ'_{ac} for a small amplitude of H_{ac} (see text). The green line represents a fit to $H_c^s(T) = H_c^s(0)[1 - (T/T_c^s)^2]$, with $\mu_0 H_c^s(0) = 34.9$ mT and $T_c^s = 1.33$ K. The blue symbols denote $H_c^R(T)$ and are taken from the superconducting transition measured by resistance. The blue line compares $H_c^R(T)$ with the WHH model curve (see text).

the ac susceptibility data measured in a small driving field $\mu_0 H_{ac} = 0.0005$ mT reported in Figs. 3(c) and 3(d). For small fields ($\mu_0 H_a \leqslant 4$ mT) the $\chi'_{ac}(T)$ data [Fig. 3(c)] show the same behavior as reported in Fig. 3(a) ($\mu_0 H_{ac} = 0.25$ mT). However, for $\mu_0 H_a \geqslant 6$ mT, the DPE peak progressively reduces and screening persists even for fields exceeding H_c. The $\chi'_{ac}(H_a)$ data [Fig. 3(d)] show that at the lowest temperature (0.31 K) screening of the full superconducting volume takes place until $\sim$17 mT. By further increasing H_a the screened volume is reduced in a stepwise fashion, until finally at 33 mT the diamagnetic signal disappears completely. Since the $\chi'_{ac}(T, H_a)$ data show a full screening signal above H_c, this signal must come from the superconducting surface layer. This also explains why the large peak due to the DPE located just below H_c becomes smaller and smaller with increasing applied field [Fig. 3(c)] or decreasing temperature [Fig. 3(d)]: The bulk is screened by the surface layer [36]. The screening efficacy of the surface layer strongly depends on the amplitude of H_{ac} (see SM [31]). In Fig. 3(a), $\mu_0 H_{ac} = 0.25$ mT and the screening is weak, while in Fig. 3(b), $\mu_0 H_{ac} = 0.0005$ mT and the screening is large. It tells us flux pinning in the surface sheath is extremely weak and can be overcome by a driving field of typically 0.25 mT.

Next, we present the superconducting phase diagram derived from the magnetic and transport measurements (Fig. 4). Superconductivity of the bulk is found below the H_c phase line. The critical field of the surface layer $H_c^s(T)$ is identified from the data in Figs. 3(c) and 3(d) by the field ($> H_c$) at which $\chi'_{ac}(H)$ or $\chi'_{ac}(T)$ reaches zero. We remark that for the small amplitude ac field, $\mu_0 H_{ac} = 0.0005$ mT, $H_c^s(T)$ is well defined due to the steplike feature when $\chi'_{ac} \to 0$. For larger amplitudes of H_{ac}, the step broadens (see SM [31]). Theory predicts that for a type-1 superconductor with $\kappa > 0.42$ the critical field

for surface superconductivity is given by $H_{c3} = 2.39 \times \kappa H_c$, while for $\kappa \leqslant 0.42$ the result is $H_{c3} < H_c$ [22,23]. For PdTe$_2$ we calculate $\kappa = 0.34$, thus H_{c3} should be absent. This implies $H_c^s(T)$ cannot be attributed to the standard Saint-James–de Gennes surface critical field for a type-1 superconductor. The extrapolation of $H_c^s(T)$ to $H \to 0$ reveals T_c^s of the surface layer is 1.33 K, which is lower than the bulk T_c (see Fig. 4). Here, we fitted $H_c^s(T)$ to a quadratic temperature function, from which we infer $\mu_0 H_c^s(0) = 34.9$ mT. Remarkably, electrical resistance measurements for $H_a \parallel a$ on the same PdTe$_2$ crystal reveal superconductivity survives up to fields that are almost a factor of 10 higher (see the right panel in Fig. 4 and SM [31] for details). The critical field determined by transport $H_c^R(T)$ tracks the $H_c(T)$ curve for low fields (see SM [31]), but increases rapidly below $\sim$1.3 K. This temperature coincides, within the error bar, with T_c^s, which strongly suggests the transport experiment probes superconductivity of the surface layer as well. The $H_c^R(T)$ curve compares quite well with the standard Werthamer-Helfand-Hohenberg (WHH) expression for a weak-coupling spin-singlet superconductor in the clean limit [37] (see SM [31]).

The phase diagram with type-I superconductivity below $T_c = 1.64$ K and surface superconductivity below $T_c^s = 1.33$ K is at odds with the standard BCS behavior, but we stress it is a robust property of our PdTe$_2$ crystals. We have performed a number of checks. First of all, SEM and EDX showed our crystals to have a homogeneous 1:2 composition and no foreign phases were detected (see SM [31]). Second, and most important, after taking the M and χ_{ac}' data we carefully polished the surfaces of the crystal and remeasured the magnetic properties with essentially the same results for the bulk and surface (see SM [31]). This provides compelling evidence that surface superconductivity is not due to an impurity phase on the surface. We emphasize the large critical field $H_c^R(T)$ measured by resistance is a robust property of our crystals as well. Resistance measurements for $B \parallel a^*$ and c axis on the same crystal, as well as on other crystals, all show similarly enhanced values of $H_c^R(T)$ (see SM [31]). The close to isotropic behavior for $B \parallel a$, a^*, and c axis indicates the superconducting transition in resistance is not due to filamentary superconductivity (see SM [31]). Finally, we remark that Fei *et al.* [2] reported a large critical field $\sim$0.32 T for $T \to 0$ deduced from resistance data, too.

The unusual superconducting phase diagram of PdTe$_2$ shows some similarities with the diagrams reported for the type-I superconductors LaRhSi$_3$ [21] and AuBe [38]. For these materials also a surface critical field much larger than H_c is found. However, in both cases it was attributed to a field-induced change from type-I to type-II/1 superconductivity below a conversion temperature $T^* < T_c$, which is possible when κ is close to $1/\sqrt{2}$ [39]. On the other hand, both LaRhSi$_3$ and AuBe have a noncentrosymmetric crystal structure. Theory predicts the lack of inversion

symmetry can possibly give rise to exotic superconducting properties due to the mixing of spin-singlet and triplet order parameters [40], as well as to unusual surface states. This possibly explains the measured critical fields are much larger than H_c. If the type-II/1 scenario would apply to PdTe$_2$, H_c^s would signal the boundary of the field-induced vortex phase H_{c2}, and H_c^R is H_{c3}. We recall that for PdTe$_2$, $\kappa = 0.34 < 1/\sqrt{2}$, and the dc magnetization data in Fig. 1, notably the small magnitude of the tail when $M(H) \to 0$, do not provide evidence for a bulk transition from type I to type II. Moreover, signatures of supercooling (see SM [31]) rule out type-II/1 superconductivity. Specific-heat measurements in applied fields would be helpful to elucidate this further [21].

The structure of superconducting states in Dirac semimetals was recently investigated by theoretical work [2,41–43]. Depending on the different pairing potentials, topological odd-parity superconductivity in the bulk with gap nodes is a possibility. Since we find that PdTe$_2$ is a conventional BCS superconductor, such a scenario is most likely ruled out. On the other hand, ARPES measurements in the normal state reveal the presence of a topological surface state [1,13]. Possibly, a superconducting gap opens in this topological surface state at T_c^s, below T_c of the bulk. Since superconductivity of the surface layer has two critical fields, H_c^s and H_c^R, and does not fit into the standard BCS picture, we speculate it could have a topological nature. This calls for an in-depth examination of superconductivity in PdTe$_2$, by, e.g., scanning tunneling probe techniques.

In summary, we have investigated the superconducting properties of the compound PdTe$_2$ that was recently reported to be a type-II Dirac semimetal. dc magnetization and ac susceptibility measurements clearly show PdTe$_2$ is a type-I superconductor with $T_c = 1.64$ K and a critical field $\mu_0 H_c(0) = 13.6$ mT. Our crystals also show the intermediate state as is demonstrated by the differential paramagnetic effect observed in the ac susceptibility. In addition, superconductivity of the surface layer is found below $T_c^s = 1.33$ K $< T_c$. It persists up to $\mu_0 H_c^s(0) = 34.9$ mT and does not follow the standard Saint-James–de Gennes behavior. Resistance data point to an even larger critical field for the surface layer $H_c^R(0) \approx 0.30$ T. PdTe$_2$ is the only topological material for which type-I superconductivity has been reported so far. This, together with the unusual superconducting phase diagram, calls for a close examination of superconductivity in PdTe$_2$, especially in view of the presence of topological surface states.

[1] H.-J. Noh, J. Jeong, E.-J. Cho, K. Kim, B. I. Min, and B.-G. Park, Phys. Rev. Lett. **119**, 016401 (2017).

[2] F. Fei, X. Bo, R. Wang, B. Wu, J. Jiang, D. Fu, M. Gao, H. Zheng, Y. Chen, X. Wang, H. Bu, F. Song, X. Wan, B. Wang, and G. Wang, Phys. Rev. B **96**, 041201(R) (2017).

[3] A. A. Soluyanov, Physics **10**, 74 (2017).

[4] C.-K. Chiu, J. C. Y. Teo, A. P. Schnyder, and S. Ryu, Rev. Mod. Phys. **88**, 035005 (2016).

[5] B. Yan and C. Felser, Annu. Rev. Condens. Matter Phys. **8**, 337 (2017).

[6] N. P. Armitage, E. J. Mele, and A. Vishwanath, arXiv:1705.01111 [Rev. Mod. Phys. (to be published)].

[7] S. M. Young, S. Zaheer, J. C. Y. Teo, C. L. Kane, E. J. Mele, and A. M. Rappe, Phys. Rev. Lett. **108**, 140405 (2012).

[8] X. Wan, A. M. Turner, A. Vishwanath, and S. Y. Savrasov, Phys. Rev. B **83**, 205101 (2011).

[9] A. A. Soluyanov, D. Gresch, Z. Wang, Q. Wu, M. Troyer, X. Dai, and B. Bernevig, Nature (London) **527**, 495 (2015).

[10] H. Huang, S. Zhou, and W. Duan, Phys. Rev. B **94**, 121117(R) (2016).

[11] M. Yan, H. Huang, K. Zhang, E. Wang, W. Yao, K. Deng, G. Wan, H. Zhang, M. Arita, H. Yang, Z. Sun, H. Yao, Y. Wu, S. Fan, W. Duan, and S. Zhou, Nat. Commun. **8**, 257 (2017).

[12] J. Guggenheim, F. Hulliger, and J. Müller, Helv. Phys. Acta **34**, 408 (1961).

[13] L. Yan, Z. Jian-Zhou, Y. Li, L. Cheng-Tian, L. Ai-Ji, H. Cheng, D. Ying, X. Yu, H. Shao-Long, Z. Lin, L. Guo-Dong, D. Xiao-Li, Z. Jun, C. Chuang-Tian, X. Zu-Yan, W. Hong-Ming, D. Xi, F. Zhong, and Z. Xing-Jiang, Chin. Phys. Lett. **32**, 067303 (2015).

[14] M. Sato and S. Fujimoto, J. Phys. Soc. Jpn. **85**, 072001 (2016).

[15] M. Sato and Y. Ando, Rep. Progr. Phys. **80**, 076501 (2017).

[16] A. Kjekshus and W. B. Pearson, Can. J. Phys. **43**, 438 (1965).

[17] C. Raub, V. Compton, T. Geballe, B. Matthias, J. Maita, and G. Hull, J. Phys. Chem. Solids **26**, 2051 (1965).

[18] Y. Wang, J. Zhang, W. Zhu, Y. Zou, C. Xi, L. Ma, T. Han, J. Yang, J. Wang, J. Xu, L. Zhang, L. Pi, C. Zhang, and Y. Zhang, Sci. Rep. **6**, 31554 (2016).

[19] L. L. Zhao, S. Lausberg, H. Kim, M. A. Tanatar, M. Brando, R. Prozorov, and E. Morosan, Phys. Rev. B **85**, 214526 (2012).

[20] S. Sun, L. Liu, and H. Lei, J. Phys.: Condens. Matter **28**, 085701 (2016).

[21] N. Kimura, N. Kabeya, K. Saitoh, K. Satoh, H. Ogi, K. Ohsaki, and H. Aoki, J. Phys. Soc. Jpn. **85**, 024715 (2016).

[22] D. Saint-James and P. G. Gennes, Phys. Lett. **7**, 306 (1963).

[23] D. Saint-James, E. J. Thomas, and G. Sarma, *Type II Superconductivity* (Pergamon, Oxford, UK, 1969).

[24] L. Thomassen, Z. Phys. Chem. B **2**, 349 (1929).

[25] S. Manzeli, D. Ovchinnikov, D. Pasquier, O. V. Yazyev, and A. Kis, Nat. Rev. Mater. **2**, 17033 (2017).

[26] H. Myron, Solid State Commun. **15**, 395 (1974).

[27] A. E. Dunsworth, J. Low Temp. Phys. **19**, 51 (1975).

[28] J.-P. Jan and H. L. Skriver, J. Phys. F: Met. Phys. **7**, 1719 (1977).

[29] M. K. Hooda and C. S. Yadav, arXiv:1704.07194.

[30] A. Lyons, D. Schleich, and A. Wold, Mater. Res. Bull. **11**, 1155 (1976).

[31] See Supplemental Material at http://link.aps.org/supplemental/10.1103/PhysRevB.96.220506 for sample characterization and additional experiments.

[32] C. P. Poole, H. A. Farach, R. J. Creswick, and R. Prozorov, *Superconductivity*, 2nd ed. (Elsevier, Amsterdam, 2007).

[33] R. A. Hein and R. L. Falge, Phys. Rev. **123**, 407 (1961).

[34] M. Tinkham, *Introduction to Superconductivity* (McGraw-Hill, New York, 1996).

[35] K. Kudo, H. Ishii, and M. Nohara, Phys. Rev. B **93**, 140505(R) (2016).

[36] J. L. Weber and J. P. McEvoy, Phys. Status Solidi B **57**, K87 (1973).

[37] N. R. Werthamer, E. Helfand, and P. C. Hohenberg, Phys. Rev. **147**, 295 (1966).

[38] D. J. Rebar, Ph.D. thesis, Louisiana State University, 2015.

[39] J. Auer and H. Ullmaier, Phys. Rev. B **7**, 136 (1973).

[40] S. Yip, Annu. Rev. Condens. Matter Phys. **5**, 15 (2013).

[41] T. Hashimoto, S. Kobayashi, Y. Tanaka, and M. Sato, Phys. Rev. B **94**, 014510 (2016).

[42] S. Kobayashi and M. Sato, Phys. Rev. Lett. **115**, 187001 (2015).

[43] G. Bednik, A. A. Zyuzin, and A. A. Burkov, Phys. Rev. B **92**, 035153 (2015).